

# Exomoon Candidates from Transit Timing Variations

## *Six Kepler systems with TTVs explainable by photometrically unseen exomoons*

Chris Fox, Paul Wiegert<sup>1</sup> 

<sup>1</sup>The University of Western Ontario, Department of Physics & Astronomy, London, Ontario, Canada

Last updated June 2020, submitted to the Monthly Notices of the Royal Astronomical Society

### ABSTRACT

If a transiting exoplanet has a moon, that moon could be detected directly from the transit it produces itself, or indirectly via the transit timing variations it produces in its parent planet. There is a range of parameter space where the Kepler Space Telescope is sensitive to the TTVs exomoons might produce, though the moons themselves would be too small to detect photometrically via their own transits. The Earth’s Moon, for example, produces TTVs of 2.6 minutes amplitude by causing our planet to move around their mutual center of mass. This is more than Kepler’s short-cadence interval of 1 minute and so nominally detectable (if transit timings can be measured with comparable accuracy), even though the Moon’s transit signature is only 7% that of Earth’s, well below Kepler’s nominal threshold.

Here we explore eight systems from the Kepler data set to examine the exomoon hypothesis as an explanation for their transit timing variations, which we compare with the alternate hypothesis that the TTVs are caused by a non-transiting planet in the system. We find that the TTVs of six of these systems could be plausibly explained by an exomoon, the size of which would not be nominally detectable by Kepler. Though we also find that the TTVs could be equally well reproduced by the presence of a non-transiting planet in the system, the observations are nevertheless completely consistent with a existence of a dynamically stable moon small enough to fall below Kepler’s photometric threshold for transit detection, and these systems warrant further observation and analysis.

**Key words:** planets and satellites: detection, methods: numerical,

### 1 INTRODUCTION

Most of the planets found by the Kepler Space Telescope have been via the transit method (Borucki et al. 2010). However, additional non-transiting planets have been discovered by examining the variability of transit timings. Gravitational perturbations between planets can result in deviations from perfectly Keplerian orbits, seen as transit timing variations (TTVs) (Agol et al. 2005; Holman & Murray 2005) which can reveal the presence of otherwise undetected planets. Here we look at eight Kepler planetary systems that exhibit TTVs, and compare the hypothesis that these TTVs are caused by another planet in the system, with the hypothesis that they are caused by a companion in orbit around the planet itself, henceforth referred to as an exomoon.

There have been previous searches for exomoons in the Kepler data. The most sophisticated is the HEK (Hunt for Exomoons with Kepler, Kipping et al. (2013, 2014, 2015)) project, which uses a photodynamical approach, modelling the expected photometric signal of an exoplanet-exomoon combination from transit to transit within

a Bayesian framework. However, no search to date has made a positive identification of an exomoon. Arguably the best moon transit candidate to date comes from the HEK project: the Kepler-1625 system (Teachey & Kipping 2018). However, alternative explanations for the signal (Heller et al. 2019; Kreidberg et al. 2019) have also been proposed, and Kepler-1625 remains an unconfirmed and controversial exomoon candidate.

This project examines a different and complementary part of parameter space. We specifically consider only exomoons that are too small to create detectable photometric (transit) signals but are large enough to create TTVs in their parent planets by displacing them with respect to their mutual center of mass. As a result, this work does not examine Kepler’s photometric data at all, and we will exclude from consideration any exomoon candidates which are large enough to be easily seen from their transit signals, tacitly assuming that these would have been seen (if present) by dedicated studies for them such as HEK. This work focuses on the TTVs produced by exomoons, but is not the first to consider them. The properties of TTVs generated by hypothetical exomoons has been explored by Sartoretti, P. & Schneider, J. (1999); Kipping (2009); Heller et al. (2016). These papers were theoretical in nature and did not

\* Contact e-mail: cfox53@uwo.ca

examine real transit curves. Szabó et al. (2013) did, however, look for exomoons in the Kepler data set using Fourier Transforms of the entire transit timing data set. No definitive exomoon detections were made.

Here we approach the search for exomoons differently than previous efforts. Rather than searching for signals via a transit or Fourier analysis, we look for systems that have significant TTVs, and then examine models where those TTVs were created by 1) another planet in the system and 2) a moon in orbit around the planet, to determine which might provide a better fit to the TTV signals. One constraint we impose on our exomoon model is that the moon’s contribution to the transit signal is small enough to remain undetected. To first order, Kepler is sensitive to transiting bodies of about the size of the Earth (Gilliland et al. 2011). We will consider a body, whether planet or moon, larger than this size to be visible as a transit in the Kepler data, or equivalently this body is above Kepler’s *photometric* sensitivity limit. Similarly, Kepler can detect TTVs of order the interval between its short-cadence observations, or about one minute (Borucki et al. 2010), which sets its ultimate TTV sensitivity limit. In practice, the TTV sensitivity limit will be set by the accuracy to which the transit timings can be determined and we will consider realistic timing errors here. However, the net result is that for many Kepler systems there is a region of parameter space where an exomoon could create TTVs that are above Kepler’s TTV sensitivity limit while having a cross-section that puts it below Kepler’s photometric sensitivity which is the scenario that we examine here.

We report on two models for each system:

- (i) the TTVs are caused by another non-transiting planet, possibly with high eccentricity or at high relative inclination
- (ii) the TTVs are caused by a single exomoon whose orbit may be eccentric but is coplanar

Initially we also examined a third case where we consider two moons orbiting the planet in circular coplanar orbits. However, as will be discussed later, this hypothesis proved to result in systems that were highly unstable and we did not find any viable two moon systems that could explain the TTV patterns better than the other two models.

Under each model, we conduct a multi-parameter search to determine the parameters that best recreate the observed TTV signal by minimizing the chi-squared difference between the model and observed transit timings. In order for the exomoon models to be considered viable the resulting cross-section of any moons must be small enough for their transit signal to be below Kepler’s photometric threshold.

## 2 THEORETICAL BASIS FOR MOON-INDUCED TTVS

We use a simplified model of a planet-moon(s) system to model planetary TTVs resulting from the moon, as illustrated in Figure 1. The planet and moon orbit their mutual center of mass. In the absence of any other influences, the center of mass of the planet-moon system will orbit their parent star with a fixed period. The transit timing of the planet is then offset by an amount that depends on the orientation of the planet-moon system during the transit. The TTV for single transit for this simple model is expressed as:

$$TTV = \left( \frac{P_p}{2\pi GM_*} \right)^{1/3} \frac{M_m a_{pm}}{M_p + M_m} \frac{(1 - e^2)}{1 + e \cos(f)} \sin \left( \omega + f - \frac{\pi}{2} \right) \quad (1)$$

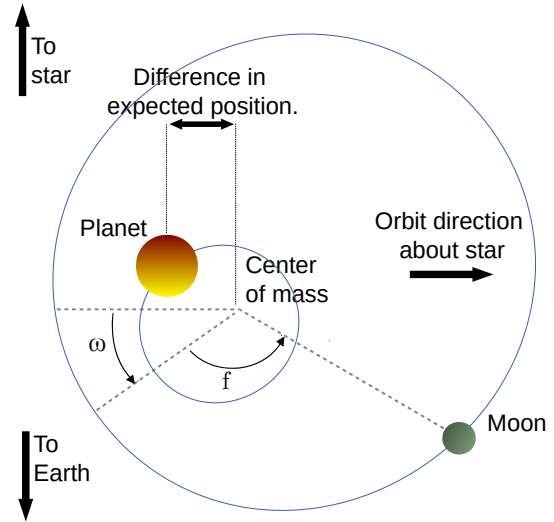
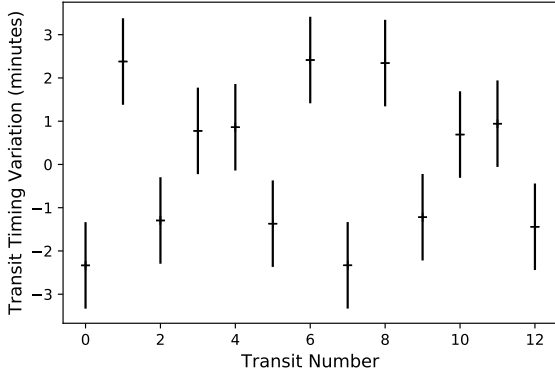


Figure 1. Simple model of planet-moon system.

where  $a_{pm}$  is the distance of the moon to the planet (not the barycentre),  $f$  the true anomaly, and  $\omega$  the argument of periastron of the moon. These definitions are consistent with those of Kipping (2009).

The moon necessarily orbits the planet with a period much shorter than the period of the planet about the star because it must orbit within the planet’s Hill sphere (Kipping 2009). Notwithstanding this, our model will assume that the period of the moon is significantly greater than the transit duration; that is that there is no motion of the planet with respect to the moon-planet center of mass during the transit. A moon on too small an orbit could produce substantial reflex motion of the planet during the transit, shortening or lengthening the transit depending on the moon’s phase. This can have an impact upon the measured transit center and timing measurement, thereby making the modelling more complex. However, we will see that in all the cases we examine here, the hypothetical moon’s period is long enough that such effects can be safely ignored.

As an example of the type of system we are examining here, applying Equation 1 to the Earth-Moon system yields a TTV amplitude of 2.58 minutes. This exceeds Kepler’s short-cadence interval of one minute so is nominally detectable. However, in practice it may not be detectable given the presence of other sources of error such as systematic and stellar noise (Gilliland et al. 2011). The Moon’s cross-section of only 7% of Earth’s puts it below Kepler’s photometric detection threshold. The Kepler Space Telescope was designed to detect an Earth-sized planet around a Sun-like star (an 85 ppm drop) with a 6.5 hour integration at  $4\sigma$ . Once on orbit, it was found that higher than expected stellar noise increased the total noise to 29 ppm, and reduced the detection confidence to  $2.7\sigma$  (Gilliland et al. 2011). We note that Earth orbits with a period of 365.26 days, which would only produce four transits in the four-year Kepler data set. For a confident detection of an exomoon, more transits would be needed. In particular, our attempts to compare models by determining the best-fit parameters require, at a minimum, one transit per parameter and ideally many more. Though our own Earth-Moon system might not be recoverable from the Kepler data set, it illustrates the principle that, in some cases, Kepler is more sensitive to TTV variations from exomoons than it is to their photometric signals. Figure 2 shows the expected TTV pattern on an Earth-Moon system with an error bar of one minute added, over



**Figure 2.** Simulated ideal TTV pattern of an Earth-Moon analog, with 1 minute error bars.

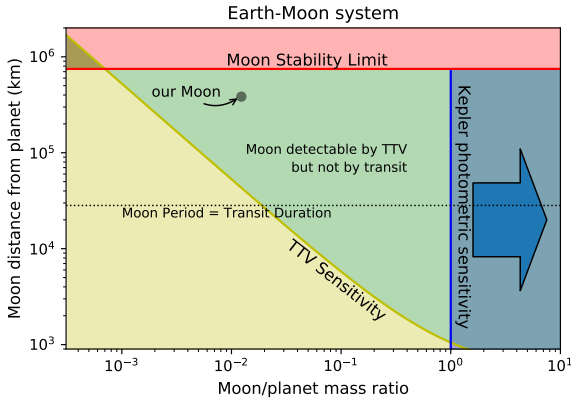


**Figure 3.** Parameter space of a Moon-Earth Analog. The diagonal line represents a TTV of 1 minute. The horizontal line represents the orbital stability of the moon at 0.5 of the Earth’s Hill radius. The vertical line is the Kepler-detection limit, using an Earth mass as proxy for an Earth radius. The grey dot indicates Earth’s Moon. Being inside the green region, our Moon would be nominally detectable by Kepler from its TTVs, but its transit would be below Kepler’s photometric sensitivity.

the course of several years providing an illustration of the possible signal in the Kepler data set.

While TTV signals of this magnitude and with low error are relatively rare in the Kepler data set, hundreds do exist. We also note that as TTV strength is linearly proportional to the moon’s mass and its semi-major axis (Equation 1), modest increases in either could produce a significantly stronger TTV signal than what is produced by the Earth-Moon system.

## 2.1 Detectability from TTVs versus Transits

Before we describe the selection criteria for our sample, it will be useful to construct a illustrative diagram of the parameter space which can be used to assess whether candidate systems are broadly consistent with our search criteria.

We define our region of interest or the ‘green zone’ to be the region where the transit signature of an exomoon would be below Kepler’s threshold of 1 Earth radius, but the planetary TTVs induced

by such moon would larger than Kepler’s short-cadence interval of one minute. Though optimistic, this detection zone provides an informative first look at the parameter space. Figure 3 illustrates the region of interest (in green) using an Earth-moon analog.

We will construct a similar but more realistic diagram for our candidate systems based on its individual stellar and planetary parameters. The lines in the diagram, which are described below, represent the approximate location of various thresholds related to our search. The green zone is the parameter space in which an exomoon could produce TTVs while being too small to be observed photometrically. Moon parameters that fall well outside of the green zone cannot and will not be considered viable exomoon candidates here because they fail to meet the criteria described below. The lines in Figure 3 and following diagrams are:

(i) Equation 2 represents Kepler’s sensitivity to exomoon-generated TTVs, expressed in terms of the moon’s parameters. This is a restatement of equation 1, assuming low eccentricity moon orbit, a fixed TTV sensitivity on the part of Kepler, and reorganized to write the moon’s distance from the planet a function of the moon-planet mass ratio.

$$a_{pm} = TTV \left( \frac{2\pi GM_*}{P_p} \right)^{1/3} \left( 1 + \left( \frac{M_m}{M_p} \right)^{-1} \right) \quad (2)$$

Equation 2 is shown by the yellow line in Figure 3 where a TTV sensitivity is 1 minute is assumed. When constructing this diagram for our target systems, we take the TTV sensitivity to be the average TTV error from Holczer et al. (2016). This is typically on the order of 3 or 4 minutes in the systems we examine, and pushes this line upwards making the green zone smaller. Any moon considered here also needs to have a preponderance of its TTV values larger than the typical TTV error, or else its TTV signal would be indistinguishable from noise: the TTV signal-to-noise is discussed in Section 3.

(ii) The red horizontal line in Figure 3, expressed by Equation 3, represents one-half of the Hill radius of the planet. This serves as our outer limit for the stability of exomoons.

$$a|_{0.5Hill} = 0.5a_p \left( \frac{M_p}{3M_*} \right)^{1/3} = 0.5 \left( \frac{G(M_* + M_p)P_p^2 M_p}{12\pi^2 M_*} \right)^{1/3} \quad (3)$$

Numerical studies have shown that prograde moons are not stable beyond about 0.3  $R_{Hill}$  (Holman & Wiegert 1999) though retrograde moons can survive out as far as 0.5  $R_{Hill}$  (Nicholson et al. 2008). As a result, any modelled fit to the TTVs that requires an exomoon above the red line would be unstable. In practice we restrict our searches to less than 0.3  $R_{Hill}$  to ensure that not only do the moons remain bound to the planet, but their orbits do not vary strongly with time (due to stellar gravitational perturbations), so that our assumption of a fixed elliptical moon orbit is valid. The use of the Hill sphere becomes questionable as the moon/planet mass approaches unity, but it provides us with a useful zeroth-order limit: any moon with an orbital radius of more than half the Hill radius is unlikely to be stable.

(iii) The blue vertical line in Figure 3, is expressed by Equation 4 and represents the Kepler transit detection limit of 1 Earth cross-section in front of a Sun-like star, expressed in terms of mass with an Earth-like density assumed. We adopt this fractional change in the photometry (85 ppm) as representative of Kepler’s photometric detection threshold for our initial survey of the parameter space.

$$\frac{M_m}{M_p} \Big|_{threshold} = \left( \frac{M_{\oplus}}{M_p} \right) \left( \frac{R_*}{R_{\odot}} \right)^2 \quad (4)$$

A moon with a mass (and hence cross-section) greater than the Earth's would appear to the right of this line, and we will consider it detectable photometrically in Kepler data. This detection limit is expressed as the moon/planet mass ratio instead of just in terms of the moon's mass for consistency with the previous equations.

This transit detection limit is affected by the star's properties, as the transit depth is inversely proportional to the square of the stellar radius. Thus, as the star's radius increases, the transit threshold line is shifted to the right. A consistent criteria for the photometric sensitivity line is used in all cases, that of a  $1R_{\oplus}$  orbiting a  $1R_{\odot}$  star, and we assume a constant planet density (that of the Earth) for simplicity. However, planets vary in radius, density, and mass. The mass is the primary driver of the entire detection space (see Equations 2, 3). Thus, while the transit detection limit line may be placed at different values of  $M_m/M_p$  for different systems, it always represents the same transit detection threshold. We note that this is not a hard limit, as Kepler has found many (146 confirmed including the K2 mission) planets of less than  $1R_{\oplus}$  and as small as  $0.34R_{\oplus}$  (Akeson et al. 2013; Stassun et al. 2017; Chen & Kipping 2018). Transit detections are subject to more factors (such as stellar noise and integration time) than we have included here. We use a  $1R_{\oplus}$  planet around a  $1R_{\odot}$  star as our first order guideline only; it is not a hard limit.

(iv) The dashed horizontal line in Fig. 3 is the distance from the planet where the moon's period is equal to the transit duration of the planet. A moon near or below this line moves significantly during the transit; however our simplified model assumes little or no motion of the moon relative to the planet during the transit. A moon near or below this line may require more advanced modelling for reasons discussed in section 2, and we will only consider systems which lie well above this line.

The four lines described above divide the parameter space in ways which will help illustrate the properties of the different modelled moon systems that will be discussed in more detail later.

## 2.2 Transit Duration Variations

Though valuable sources of information, TTVs from exomoons are subject to a degeneracy between the mass and semi-major axis of the exomoon. Transit Duration Variations (TDVs) can be brought to bear to resolve this degeneracy (Kipping 2009; Heller et al. 2016) and we incorporated the TDVs provided by Holczer et al. (2016) as part of our exomoon analysis.

All TDVs were found to be very small in comparison to their error. The ratio of standard deviation of the TDVs to the average error of the TDVs is typically just above 1 (see Table 3 later in Section 3). While small, these TDVs may still be useful by providing constraints; any proposed model that would create a large TDV could be ruled out. The TDV signal is given as a fractional value, and can be described by:

$$\frac{TDV}{\langle D \rangle} = \frac{P_p M_m}{2\pi a_p} \left[ \left( \frac{G}{(M_p + M_m)} \right) \frac{1 + e^2 + 2e \cos f}{a_{pm}(1 - e^2)} \right]^{1/2} \cos \theta \quad (5)$$

where  $\theta = \omega + f - \phi$ , and  $\phi = \arctan\left(\frac{1+e \cos f}{e \sin f}\right)$ ,  $a_{pm}$  is the semi-major axis of the planet-moon (not moon-barycentre) orbit,  $a_p$  is the semi-major axis of the planet around its parent star,  $f$  is the true anomaly of the moon about the planet, and  $\omega$  the argument of periastron of the moon's orbit. This equation is consistent with the derivation by Kipping (2009). For comparison, our Moon produces a fractional duration variation upon Earth of 0.000418.

## 3 TARGET SELECTION

To find a list of targets for analysis, we first searched for systems with TTVs with the potential to be induced by an exomoon, but only those where the exomoon's size was below Kepler's nominal detection threshold. All planets were required to have a disposition of "confirmed" or a disposition score of 1 from NASA's Exoplanet Archive (Akeson et al. 2013). Further, all planets chosen did not have any known siblings.

To first reduce the entire data set, we compute the maximum TTV that could be induced by an exomoon and exclude systems exceeding this limit. Equation 1 can be recast, placing the moon at maximum separation (0.3 Hill radii, based on the stability discussion in Section 4.2) and applying Kepler's 3rd Law. We assume zero eccentricity and maximum deflection, so that the sine term is unity.

$$TTV_{max} \approx \frac{0.3P_p}{2\pi} \left( \frac{M_m}{M_p + M_m} \right) \left( \frac{M_p}{3M_*} \right)^{1/3} \quad (6)$$

Equation 6 expression gives us a strong initial guideline for the maximum exomoon-generated TTV that could be induced upon a planet for a given period and masses of moon, planet, and star. For this calculation, we assume a stellar mass of  $1M_{\odot}$  for simplicity, and because we are searching for systems where the moon is nominally undetectable, we set the mass of the moon to  $1M_{\oplus}$ . The maximum for this equation occurs when the mass of the planet is also  $1M_{\oplus}$ . The only remaining value required is the planetary period about the star. Here we will let the need for a sufficient number of transits to fit the parameters of our models set this limit. The planet hypothesis has the most free parameters (10). As a result, we require a minimum of 10 Kepler-observed transits so as to provide sufficient constraints to that model. Given Kepler's primary mission lifespan,  $\geq 10$  transits corresponds to a period of approximately 160 days or less (assuming no missing transits in the data). This condition effectively restricts our candidates to hotter planets orbiting relatively close to their star.

Applying the period of 160 days and masses of  $1M_{\oplus}$  (for both moon and planet) and  $1M_{\odot}$  to Equation 6, produces a value of approximately 1 hour. However, when dealing with a limited number of transits we cannot be certain whether the maximum projected separation is captured. As a moon-induced TTV curve is expected to be sinusoidal, the standard deviation of the TTVs is related to the amplitude of the TTV curve by a factor of  $\sqrt{2} \approx 1.4$ . Thus, when searching the Kepler data set we limited our targets to those planets whose TTV signal has a standard deviation of 40 minutes or less. This yields 943 targets.

Next we used the physical properties for each of the individual target planets to estimate the minimum required moon mass that could theoretically produce the TTV signal for that specific planet. If this moon was too large it would be detectable photometrically and was excluded from our sample. We correlated the data from Holczer et al. (2016) for the TTV strength (standard deviation of 40 minutes or less) with the planetary mass estimates from Chen & Kipping (2018) and the stellar information from Akeson et al. (2013). From Equation 6 we solved for the mass of the moon and estimated its radius (using an Earth-like density). It is the combined size of moon and star that determines the transit depth, which we compared to an Earth-Sun transit equivalent. If the ratio was  $\approx 1$  (corresponding to a transit depth of 85 ppm) or less it made our target shortlist, otherwise it was discarded. This left us with 110 candidates.

The final criterion is provided by the signal-to-noise of the TTV signal. Here we define the signal-to-noise of the TTVs to be the ratio of standard deviation of the TTVs to their average uncertainty, as

**Table 1.** Measured Properties of Target Systems

KOI ID	Kepler ID	Spec Type	Star Mass ( $M_{\odot}$ )	Star Radius ( $R_{\odot}$ )	Transit Depth (ppm)
268.01		F7*	$1.175^{+0.058}_{-0.065}$	$1.359^{+0.062}_{-0.068}$	$489.8 \pm 5.2$
303.01	517b	G6V	$0.871^{+0.071}_{-0.043}$	$1.023^{+0.142}_{-0.142}$	$755.6 \pm 7.3$
1503.01	867b	G3*	$0.916^{+0.062}_{-0.056}$	$0.943^{+0.123}_{-0.082}$	$2378.5 \pm 37.2$
1888.01	1000b	F6IV	$1.406^{+0.086}_{-0.086}$	$1.467^{+0.24}_{-0.111}$	$886.0 \pm 21.6$
1925.01	409b	K0	$0.902^{+0.050}_{-0.055}$	$0.888^{+0.036}_{-0.036}$	$123.3 \pm 4.8$
1980.01	1036b	G5	$0.875^{+0.054}_{-0.049}$	$0.861^{+0.088}_{-0.051}$	$717.7 \pm 19.7$
2728.01	1326b	F4IV*	$1.535^{+0.219}_{-0.267}$	$2.632^{+0.471}_{-0.875}$	$512.6 \pm 19.3$
3220.01	1442b	F7*	$1.323^{+0.098}_{-0.088}$	$1.401^{+0.263}_{-0.132}$	$762.3 \pm 16.1$

All values from NASA's Exoplanet Archive (Akeson et al. 2013), except Spectral Types are from Simbad (Wenger et al. 2000). Spectral Type values indicated with an \* are estimates based on effective temperature.

derived from Kepler observations by Holczer et al. (2016). These quantities are calculated with all identified outliers removed, and in particular the measured uncertainties in the transit timings are used, not any theoretical value derived from the short-cadence timing interval.

The candidates with the highest SNR were selected for further analysis. Even the top candidates have rather low SNR values, with the top ten ranging from somewhat above 2 down to 1.5. These values are low, but this arises essentially by construction of our sample. We deliberately exclude large moons because they would be photometrically detectable, leaving us the smallest (and therefore noisiest) candidates. In addition, our definition of SNR is conservative. The standard deviation is used here as a proxy of the signal, but a sinusoid (the expected signal from a moon on a circular orbit) has an amplitude which is  $\sqrt{2} \approx 1.4$  times its standard deviation. Our SNR values are thus an underestimate and serve here primarily as a guide to selecting our sample. In short, the signals from our searched-for exomoons are *a priori* expected to be weak, and we do indeed find them to be. The strongest of these signals are selected for further analysis below.

We found 8 systems, with a diverse range of stellar masses and planetary radii, masses, and periods, summarized in Table 1. At this point, these systems have only the potential to exhibit TTV behavior from an exomoon based on the observed amplitude and required mass / radius. Whether the TTV / TDV pattern is reproducible would be determined by our simulations.

## 4 METHODS AND SETUP

### 4.1 Simulating Systems and Finding Parameters

To examine the hypothesis that the TTVs and TDVs observed by Kepler were produced by an exomoon, we developed code to compute the TTVs and TDVs induced by either one or two exomoons in orbit around the planet. Our analysis also employed two publicly available software packages. The first was TTVFast (Deck et al. 2014) which simulates the orbits of the planets around a star and calculates the TTVs resulting from planetary gravitational inter-

**Table 2.** Planet Properties Estimates

KOI	Radius ( $R_{\oplus}$ )	Mass ( $M_{\oplus}$ )	Average Period (days)	Avg TTV Error (min)
268.01	$3.02^{+0.14}_{-0.14}$	$9.33^{+7.65}_{-4.08}$	$110.37838 \pm 0.00069$	3.10
303.01	$2.57^{+0.42}_{-0.23}$	$7.59^{+6.21}_{-3.42}$	$60.92833 \pm 0.00018$	3.11
1503.01	$4.68^{+0.57}_{-0.41}$	$20.42^{+16.74}_{-9.20}$	$150.24188 \pm 0.00011$	6.67
1888.01	$4.68^{+0.57}_{-0.51}$	$19.95^{+16.36}_{-8.99}$	$120.01918 \pm 0.00065$	5.21
1925.01	$1.0^{+0.05}_{-0.05}$	$1.00^{+0.78}_{-0.34}$	$68.95832 \pm 0.00045$	5.01
1980.01	$2.45^{+0.24}_{-0.22}$	$6.92^{+5.38}_{-3.03}$	$122.88122 \pm 0.00156$	10.74
2728.01	$5.25^{+1.51}_{-0.98}$	$24.55^{+26.74}_{-11.96}$	$42.35120 \pm 0.00035$	7.26
3220.01	$3.80^{+0.57}_{-0.41}$	$14.13^{+12.17}_{-6.37}$	$81.41635 \pm 0.00042$	4.68

Periods and average TTV errors computed using data from Holczer et al. (2016). Radius and Mass estimates (including  $1\sigma$  errors) from Chen & Kipping (2018)

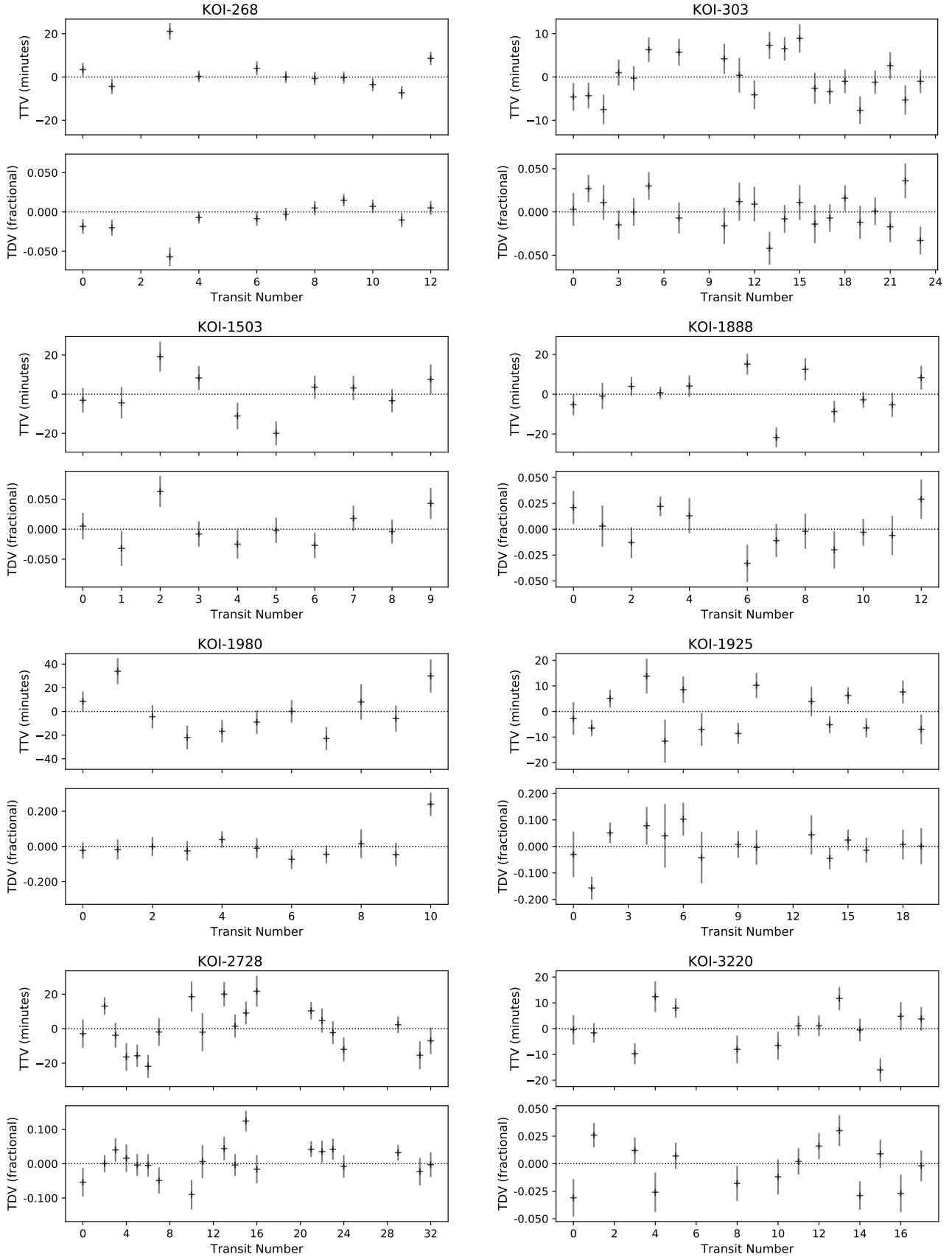
**Table 3.** Signal to Noise of Target Systems TTVs and TDVs

KOI	TTV Std Dev (min)	TTV Avg Err (min)	TTV SNR	TDV Std Dev (min)	TDV Avg Err (min)	TDV SNR
268.01	7.33	3.10	2.37	0.019	0.009	2.158
303.01	4.85	3.11	1.56	0.020	0.018	1.082
1503.01	10.4	6.67	1.56	0.031	0.023	1.333
1888.01	9.56	5.21	1.84	0.019	0.016	1.125
1925.01	7.87	5.01	1.57	0.061	0.064	0.961
1980.01	18.13	10.74	1.69	0.084	0.058	1.441
2728.01	12.38	7.26	1.71	0.045	0.035	1.305
3220.01	7.82	4.68	1.67	0.021	0.014	1.482

All values computed from Holczer et al. (2016) data.

actions. This code was used to assess the competing hypothesis that the observed TTVs were induced by a non-transiting planet. The second package was MultiNest (Feroz et al. 2009), (which we used via its Python interface, PyMultiNest (Buchner et al. 2014)), a Bayesian Inference tool which we used to search the parameter space for possible solutions for both the exomoon and exoplanet hypotheses.

For each system, the observed transit times and durations come from Holczer et al. (2016). The quality of fit for each simulation is based on the usual  $\chi^2$  value, which is converted to a log-likelihood value for MultiNest. For the exomoon hypothesis, both the TTVs and TDV were fitted. For the exoplanet hypothesis only the TTVs were fitted, as these were sufficient to demonstrate the plausibility of an additional planet as a competing hypothesis. Posteriors and best-fit parameters were exported from MultiNest. Both the best-fit values and posteriors are shown on the sensitivity plots, while the TTV and TDV plots show the pattern produced by the best-fit values.

**Figure 4.** Transit Timing Variations (TTVs) and Transit Duration Variations (TDVs) of Target Systems.

## 4.2 System Stability

As part of our analysis, systems that showed good TTV and/or TDV fits were further tested for long-term stability. The stability simulation codes used different algorithms for the case where only planets were included, and ones that included moons. The code used for the purely planetary case is a symplectic one based on the Wisdom-Holman algorithm (Wisdom & Holman 1991). This code uses a timestep less than 1/20th of the period of the innermost planet in all cases, and includes post-Newtonian general relativistic effects. This is the same code as used in Fox & Wiegert (2019). In cases where the stability of moons is examined, the RADAU15 (Everhart 1985) algorithm is used, with a tolerance of  $10^{-12}$ .

These stability studies provide an additional check on our results, as some planet and/or moon parameter values which provide good matches to the TTVs over the course of Kepler's lifetime may be unstable on longer times, and are thus unlikely to represent the real configuration of these systems. All planet hypothesis results discussed in this work were found to be in stable configurations over 10 million years, so we cannot exclude the additional planet hypothesis on the basis of system instability. The single-moon hypothesis results were all found to be stable for at least 100 (Earth) years, which corresponds to 300,000 to 5 million moon orbits, depending on the system.

Stability is of particular concern with regards to the two-moon models. The analyses of Gladman (1993) and Chambers et al. (1996) on the stability of multi-planet systems are likely approximately applicable here. Even though the stability of moons is really quite a different problem, our restriction to moons orbiting inside  $0.3 R_{Hill}$  means that stability results for planetary systems are likely to provide a useful guide. Those authors find that stability (more precisely Hill stability, that is the absence of close encounters, but in practice these encounters result in the ejection of one or both of the moons) of a two moon system is only expected where the moons are more than  $2\sqrt{3}$  mutual Hill radii apart. Combining the planetary  $0.3 R_{Hill}$  condition with the lunar  $2\sqrt{3}$  mutual Hill radii results in a significant restriction to our model. The need for the moon to generate significant TTVs tends to favour models with a large moon near  $0.3 R_{Hill}$ , and the resulting large mutual Hill radius forces the second moon to be very near the planet. The TTVs then are primarily driven by the outer moon, not dissimilar to the single moon scenario and providing little improvement to the fit. In addition, this configuration always proved to be rapidly unstable. While multiple exomoons could certainly exist around exoplanets, the size required to produce the TTVs of our sample systems preclude the existence of multiple *massive* moons, and we do not examine the multiple moon scenario further.

## 4.3 Parameters and Priors

The two models (exomoon vs additional planet) have a different set of priors and allowed parameter ranges. The mass of the known transiting planet is taken to be fixed in both cases, with the nominal mass ( $0 \sigma$ ) taken from Chen & Kipping (2018).

### 4.3.1 Exomoon hypothesis priors

When considering the planet-moon interactions, the planet is taken to have a circular orbit around the star. The moon is assumed to orbit the planet in the same plane that the planet does the star; any differences between these planes results in a mass-inclination degeneracy. Thus, our derived mass results can be considered as

minimum masses. The moon is also taken to orbit in the same (prograde) direction as the planet. Similar TTVs and TDVs could be created by a retrograde moon and such moons could be stable out to larger radii (see Section 2.1). Nevertheless, we choose prograde moons as the more likely and more conservative assumption, since we cannot distinguish the two cases from our data.

The other parameters are the mass of the moon, its semi-major axis, mean anomaly, eccentricity, and argument of periastron, for a total of 5 parameters. The moon is allowed to have a non-circular orbit, but stellar gravitational perturbations are ignored; its orbit is considered fixed. The stability simulations of exomoon candidates (discussed in Section 4.2 and 5) showed only small changes to the moon orbits during the time examined, so this assumption is valid.

For the moon hypotheses, the moon mass prior was uniform from zero though to a maximum value equal to the planet's mass. While this choice runs against some of our actual prior knowledge about the system, that is, that moons have not been detected photometrically within them despite extensive searches, it ensures we cover the full range of possible masses. Because of the degeneracy between the moon's mass and semi-major axis, we represent the greater likelihood of a smaller and farther-out moon through a triangular prior on the semi-major axis. Such a prior also assists in keeping the moon above the duration-period limit where our model would break down. This triangular semi-major axis prior has a probability density of 0 at 0 radii, and a linearly increasing probability density up to a maximum at  $0.3 Hill$  (this latter limits chosen for reasons of stability as discussed in Section 2.1). Note that this choice of prior does not affect the quality (that is, the  $\chi^2$ ) of any particular fit, though it does bias MultiNest's choices and the resulting posteriors towards larger  $a_{pm}$ .

The prior distributions for the remaining moon orbital elements were all uniform. Eccentricity was allowed to go as high as 0.5, and the angular elements could run from 0 to 360 degrees.

### 4.3.2 Exoplanet hypothesis priors

When considering planet-planet interactions, there are a total of 10 parameters. Each planet has 7 parameters: 6 orbital elements plus its mass. The known transiting planet has 3 parameters known to high precision: the period, inclination and longitude of the ascending node. The average period is known, and we use a fixed mass, the nominal value from Chen & Kipping (2018). The inclination (with respect to the planet of the sky) must be near  $90^\circ$  or else a transit would not be observed. Slight deviations in inclination have minimal effect on the observed TTVs (Agol et al. 2005) so we set the inclination to  $90^\circ$  for the known planet. Finally, the longitude of the ascending node, while not known in a true sense, can be set as our reference orientation of  $0^\circ$ , leaving 3 orbital elements. The second hypothesized new planet has nothing known about it, so it has 7 parameters to be fit: 6 orbital parameters plus its mass. This means a total of 10 parameters to fit the additional planet hypothesis. In all cases, the proposed new planet was permitted to have periods from a 1 day period to more than 4:1 resonance outside of the known planet, and a mass prior up to  $1500 M_{\oplus}$  (approximately 5 Jupiter masses).

## 5 RESULTS

Each hypothesis (moon and planet) was run at least 3 times for each system. We include both the best-fit results as well as the Bayesian posteriors for the runs that produced the lowest  $\chi^2$ . Each

run (for planet and moon hypotheses) also had to be stable in our long term simulations. Configurations that were not stable were disregarded, but all exomoon and additional planet models reported on here proved dynamically stable over the time scales tested. The observed TTVs, TDVs and associated errors for the eight systems selected [Holczer et al. \(2016\)](#) are shown in Figure 4. Comparison of the modelled TTVs with the observations are shown separately for each candidate (in order of KOI number) below.

Full results for both best fit parameters and Bayesian posteriors are included in the appendix.

### 5.1 KOI-268

Spectral Type	F7	Planet Period	110.38 d
Star Radius	$1.36 R_{\odot}$	Planet Radius	$3.0 R_{\oplus}$
Star Mass	$1.18 M_{\odot}$	Planet Mass	$9.3 M_{\oplus}$
		Avg TTV Err	3.1 min

KOI-268 is our only unconfirmed target (and hence has no Kepler designation), but has a disposition score of 1 from NASA’s Exoplanet Archive ([Akeson et al. 2013](#)), indicating there is high confidence that this is an actual planet. It is tied with KOI-303 for the lowest average TTV error, and shows the highest SNR (standard deviation / average error) in both its TTVs and TDVs.

The additional planet hypothesis produces a far better TTV fit than the moon hypothesis, with a reduced  $\chi^2$  value of nearly 0.6 compared to 1.5. However, much of the difference in these values is attributable to a single data point, transit 3, which shows a particularly large TTV value more than double any other point. Similarly, this transit also produces an abnormally low TDV. Neither hypothesis can recover this point, but the planet simulation gets significantly closer to the TTV than the moon simulation. The best fit moon is nearly  $1 M_{\oplus}$  in size, but due to this star’s large size, the moon is well below Kepler’s photometric sensitivity and in the green zone of the sensitivity plot (Figure 5). Because our planet fit is superior to the moon fit, we conclude that the TTVs of KOI-268.01 are probably caused by a sibling planet, but given that both hypotheses give reduced  $\chi^2 \sim 1$ , the possibility of a moon as the cause cannot be ruled out.

### 5.2 KOI-303

Spectral Type	G6V	Planet Period	60.93 d
Star Radius	$1.02 R_{\odot}$	Planet Radius	$2.6 R_{\oplus}$
Star Mass	$0.87 M_{\odot}$	Planet Mass	$7.6 M_{\oplus}$
		Avg TTV Err	3.1 min

KOI-303.01 (Kepler-517b) has the smallest TTV amplitude of our candidates, with no TTV greater than 10 minutes from its average orbital period. It, along with KOI-268, has the lowest average error in the TTV data, at only 3.1 minutes. The TDV signal is essentially flat, with a SNR of 1.1.

We find that both hypotheses can provide excellent fits, with reduced  $\chi^2$  values less than 1. The moon hypothesis requires a moon mass of approximately  $0.36 M_{\oplus}$  at an orbital distance of  $0.28 R_{Hill}$ . At that mass, assuming a bulk density equal to Earth, the expected radius of this moon would be  $\approx 0.65 R_{\oplus}$ , putting it in the green zone as shown on the sensitivity plot (Figure 6). Like KOI-268, the posterior mass suggests an even lower value. We conclude that the TTVs of KOI-303.01 are equally well explainable by a moon as a sibling planet.

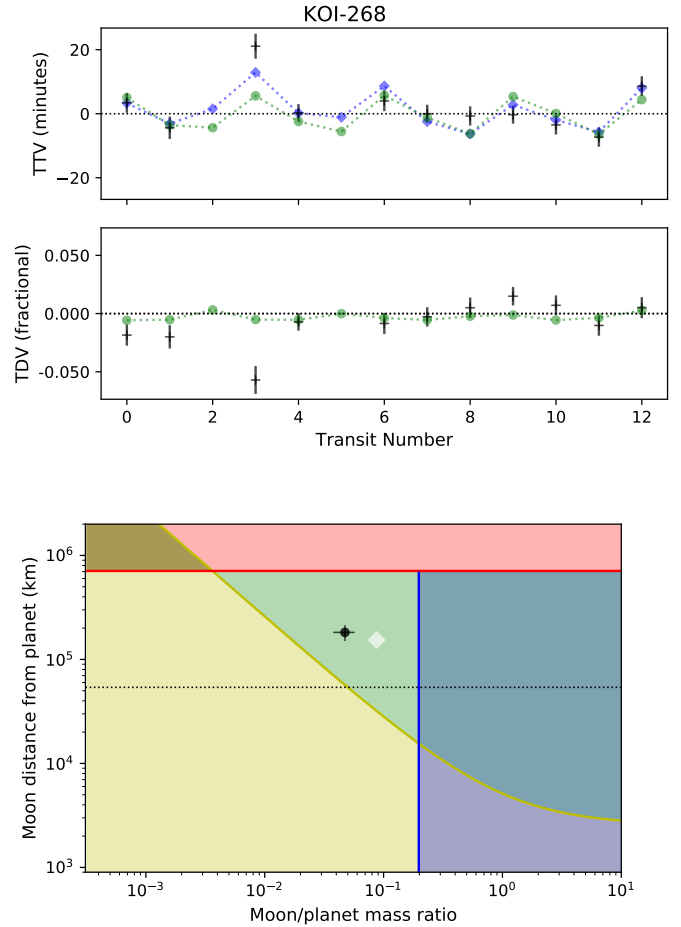


**Figure 5.** Quality of fit and sensitivity plot for KOI-268.01

In the TTV and TDV plots, the black points are the observed TTVs from Kepler (including error), the blue diamonds show the model results of the planet hypothesis and green dots indicate those for the moon hypothesis. In the sensitivity plot, the white diamond is the Best-Fit solution and the black dot is the posterior with  $1\sigma$  error.

### 5.3 KOI-1503

Spectral Type	G3	Planet Period	150.24 d
Star Radius	$0.94 R_{\odot}$	Planet Radius	$4.7 R_{\oplus}$
Star Mass	$0.92 M_{\odot}$	Planet Mass	$10.5 M_{\oplus}$
		Avg TTV Err	6.7 min

KOI-1503.01 (Kepler-867b) is a confirmed planet. Though nearly identical to KOI-1888 in estimated size and mass, 1503 produces by far the greater transit depth, 2.5x that of 1888. This is because it orbits a much smaller star. Its host star is the most Sol-like star of our sample, only slightly smaller and cooler than our sun. KOI-1503 also has our longest period, and thus the fewest number of orbits, just meeting our minimum requirement of 10 transits.

Both the planet and moon hypotheses produce good matches with the observed data. While the reduced  $\chi^2$  value is significantly better for the planet case than the moon (0.18 and 0.63 respectively). The very small value for the planet may indicate ‘over-fitting’ (either too many parameters or underestimated errors). The small star size and high uncertainties collude to produce our smallest green zone. The moon hypothesis has a best-fit mass is 1.5 Earth. As indicated on the sensitivity plot (Figure 7), such a moon should produce a clear

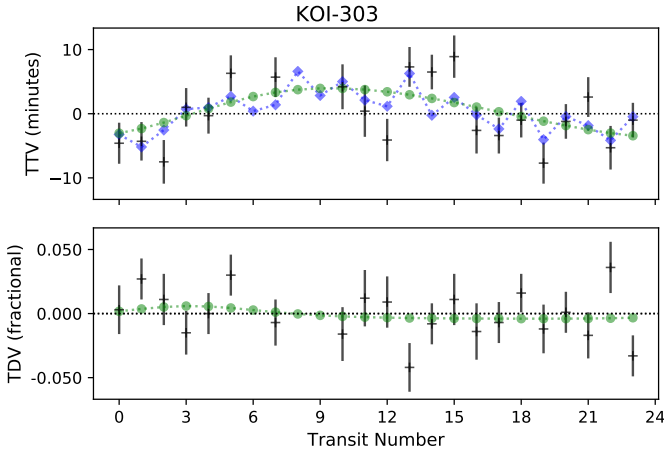


**Figure 6.** Quality of fit and sensitivity plot for KOI-303.01  
The symbols used are the same as in Figure 5.

transit signature, but we find no such signal in the publicly available data (Akeson et al. 2013). However, the posterior results suggest the possibility of a smaller moon, farther out from the planet. In this case, the signal would be near the detection threshold and may still be detectable. We conclude the TTVs of KOI-1503.01 are mostly likely due to a second planet, but an exomoon remains a possibility.

#### 5.4 KOI-1888

Spectral Type	F6IV	Planet Period	120.02 d
Star Radius	1.47 $R_{\odot}$	Planet Radius	4.7 $R_{\oplus}$
Star Mass	1.41 $M_{\odot}$	Planet Mass	20.0 $M_{\oplus}$
		Avg TTV Err	5.2 min

KOI-1888.01 (Kepler-1000b) is a confirmed planet orbiting a sub-giant F star. The planet is a near-twin to KOI-1503b, though this is has a shorter period and has better timing precision.

The TTV pattern has our second highest SNR, but the TDV pattern is among the lowest. We obtained excellent fits from both hypotheses. The planet’s reduced  $\chi^2$  is a bit higher than the moon’s (0.88 vs 0.68), but both are less than 1. The best-fit moon is 1.5 Earth in mass, and in conjunction with the sub-giant star, the best-fit moon is inside the green zone of the sensitivity plot (Figure 8). The posterior places the moon at slightly smaller mass, farther

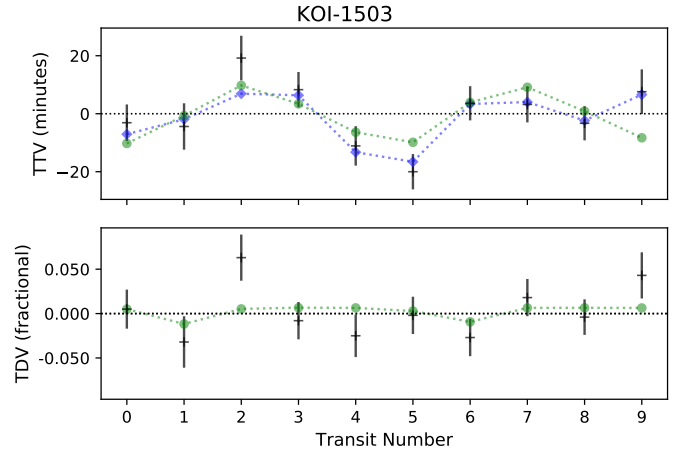


**Figure 7.** Quality of fit and sensitivity plot for KOI-1503.01  
The symbols used are the same as in Figure 5.

inside the green zone. Thus we conclude this TTV signal could be caused either by moon or planet.

#### 5.5 KOI-1925

Spectral Type	K0	Planet Period	68.96 d
Star Radius	0.89 $R_{\odot}$	Planet Radius	1.0 $R_{\oplus}$
Star Mass	0.90 $M_{\odot}$	Planet Mass	1.0 $M_{\oplus}$
		Avg TTV Err	5.0 min

KOI-1925.01 (Kepler-409b) is our sole candidate that is truly comparable to Earth in size and mass, with nominal values of 1.0 Earth in both values (Chen & Kipping 2018). Because this planet is easily the smallest of our candidates the transit depth of this system is also the least, at 0.012% (120 ppm). Only 2 of the 15 TTVs is inside of  $1\sigma$  of the TTV error, but the TDVs are mostly flat. The reduced  $\chi^2$  values are less than 1 for both planet and moon hypotheses (0.66 and 0.62 respectively). Our algorithm found the best-fit moon mass of about 0.3  $M_{\oplus}$  in a close orbit just over 0.2 Hill. As the planet is only 1  $M_{\oplus}$ , this would constitute something approaching a binary planet. However, as the posteriors show there is a wide range of possible masses below this value. If this moon’s mass was near the lower end of the posterior, then it would be proportional in mass to Earth as Charon is to Pluto (0.13 versus 0.12). This is our smallest potential moon, though would still be significantly larger than our own moon by a factor of 10.

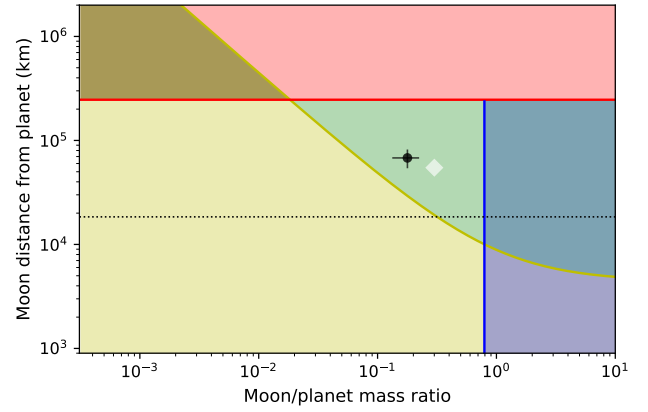
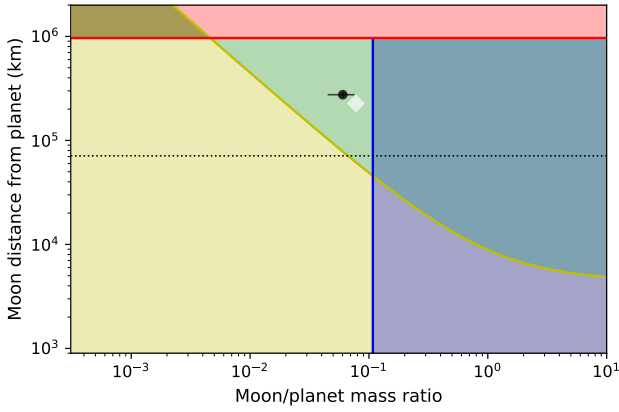
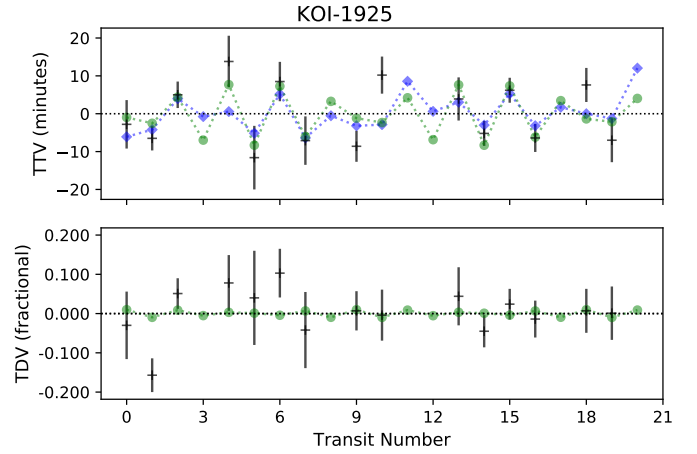
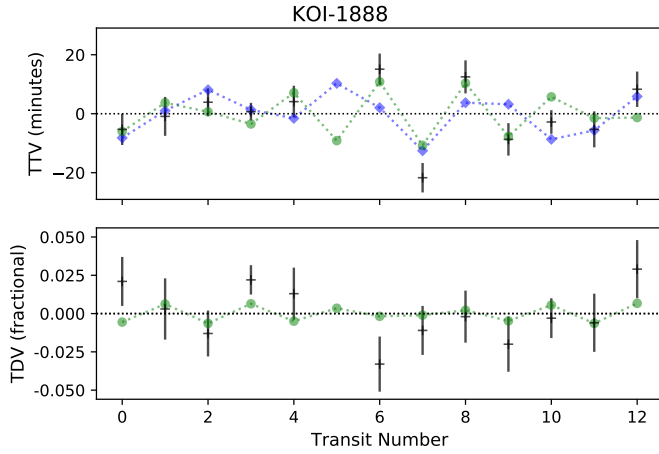


**Figure 8.** Quality of fit and sensitivity plot for KOI-1888.01  
The symbols used are the same as in Figure 5.

**Figure 9.** Quality of fit and sensitivity plot for KOI-1925.01  
The symbols used are the same as in Figure 5.

We conclude that a moon is a legitimate hypothesis, but the planet hypothesis is just as compelling.

### 5.6 KOI-1980

Spectral Type	G5	Planet Period	122.88 d
Star Radius	$0.86 R_{\odot}$	Planet Radius	$2.5 R_{\oplus}$
Star Mass	$0.88 M_{\odot}$	Planet Mass	$6.9 M_{\oplus}$
		Avg TTV Err	10.7 min

KOI-1980.01 (Kepler-1036b) is mini-Neptune sized world. It has the worst average TTV error of our sample (nearly 11 minutes), but the large TTV signal (amplitude of  $\approx 30$  minutes) mitigates this disadvantage. This system has the second-strongest TDVs signal statistically, but this appears to be caused by a single point. The TDV pattern is very flat except for one strong spike at transit 10. Like KOI-1503, this system has a very small green zone zone. In the case of -1503 this small zone is due to the planet’s mass, and in -1980 the high TTV error is the cause.

Both the planet and moon hypothesis can be satisfied with fits having reduced  $\chi^2$  values of less than 1 (0.31 and 0.64 respectively). However, the best-fit places the moon at  $0.18 R_{Hill}$  with a mass of  $2 M_{\oplus}$ . This puts the moon well to the right of the photometric transit detection threshold on the sensitivity plot (Figure 10). A cursory look of the public transit data shows no obvious indication of anything other than a single planetary transit (Akeson et al. 2013).

However, the posterior results puts the mass right at the edge of the detection limit. Even if forced to maximum distance of  $0.3 R_{Hill}$  (and minimum mass), the moon would need to be approximately Earth-massed to reproduce the observed TTV amplitude, and thus we’d expect to be able to see this in the transit curve. All combined, we conclude these TTVs are likely induced by another planet.

### 5.7 KOI-2728

Spectral Type	F4IV	Planet Period	42.35 d
Star Radius	$2.63 R_{\odot}$	Planet Radius	$5.3 R_{\oplus}$
Star Mass	$1.54 M_{\odot}$	Planet Mass	$24.6 M_{\oplus}$
		Avg TTV Err	7.3 min

KOI-2728.01 (Kepler-1326b) is the most extreme of our sample in several categories. The host star is the hottest and most massive of our candidates and has a significantly larger radius than any other. The planet is the largest in estimated radius and mass and has the shortest orbital period of our candidates. Because of the star’s extreme size, this massive planet gives the third-lowest transit depth of our sample.

The reduced  $\chi^2$  values for both planet and moon hypotheses are well below 1 (0.43 and 0.75 respectively). One system’s planet is another system’s moon: the best-fit moon is Super-Earth sized, at  $6 M_{\oplus}$ , suggesting it may be similar in size to our planet KOI-1980. But the sub-giant nature of the star, with a radius more than

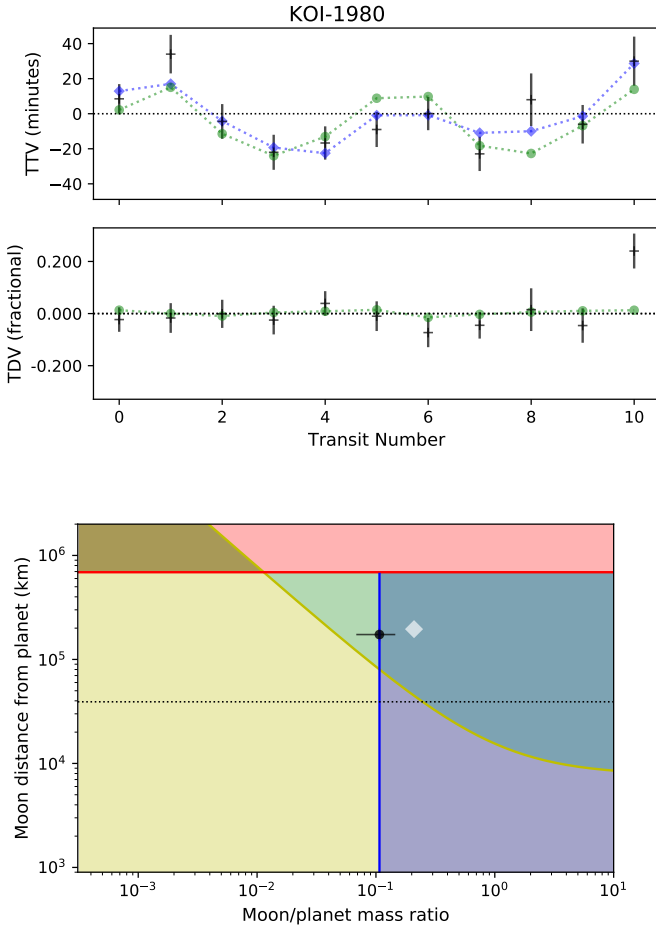


**Figure 10.** Quality of fit and sensitivity plot for KOI-1980.01  
The symbols used are the same as in Figure 5.

2.6 times that of our sun, reduces the transit signature so much that this body is just below the nominal transit detection zone. The best-fit data places the moon near the photometric detection limit, suggesting that it may be detectable but at a lower confidence level. Further, this proposed moon is as small as it can be, residing at a distance just shy of  $0.3 R_{Hill}$  limit. We conclude these TTVs could be induced either by a massive moon or by a sibling planet.

### 5.8 KOI-3220

Spectral Type	F7	Planet Period	81.42 d
Star Radius	$1.4 R_{\odot}$	Planet Radius	$3.8 R_{\oplus}$
Star Mass	$1.3 M_{\odot}$	Planet Mass	$14.1 M_{\oplus}$
		Avg TTV Err	4.7 min

KOI-3220.01 (Kepler-1442b) is another planet around a large hot star. The planet our second largest candidate, and seems to be a twin of Uranus ( $3.8 R_{\oplus}$  and  $14 M_{\oplus}$ ). Its period of 81 days is right in the middle of our sample. This planet shows a TTV pattern similar to KOI-1925.01, but with slightly lower error (4.6 vs 5.0 minutes). Unlike -1925, the TDV pattern of -3220 is one of the strongest, showing significant scatter across the entire range of data points.

The reduced  $\chi^2$  values for both hypotheses are well below 1, at 0.57 and 0.83 for the planet and moon hypotheses respectively. The moon hypothesis requires a mass of just over  $1.6 M_{\oplus}$ , residing at a distance of  $0.2 R_{Hill}$ . Against a sun-sized star, these moons would

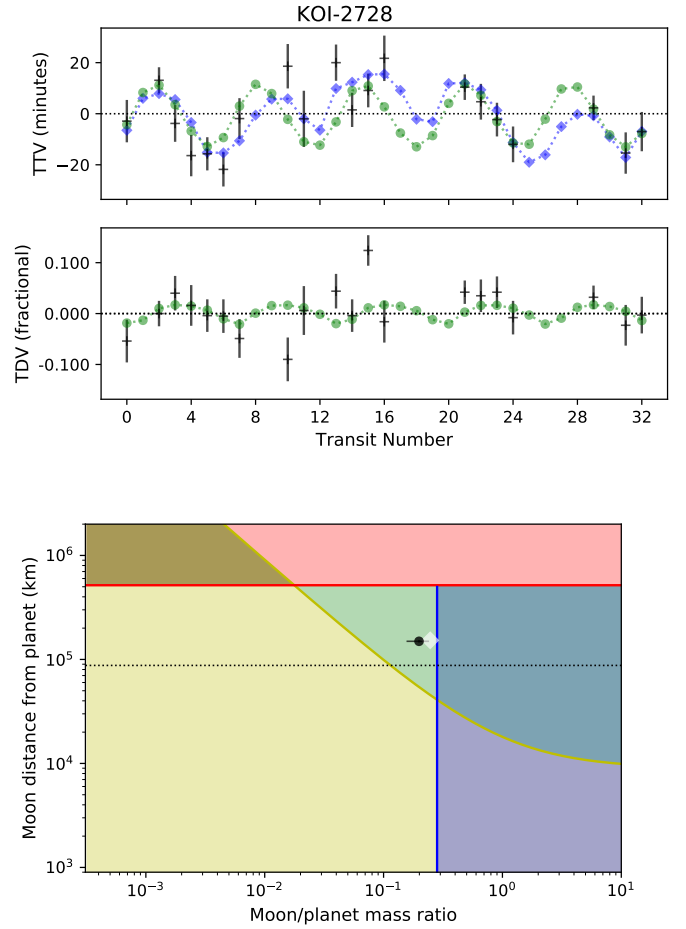


**Figure 11.** Quality of fit and sensitivity plot for KOI-2728.01  
The symbols used are the same as in Figure 5.

produce discernible transits, but this  $1.4 R_{\odot}$  star cuts the transit depth by a factor of 2. This pushes the transit detection limit to the right, and the moons end up in the green zone of the sensitivity plot (Figure 12). The best fit is near the threshold, and a cursory look at the public data (Akeson et al. 2013) gives no indication of a transit. However, the posteriors indicate a smaller moon farther out is possible, and it is would be well below the nominal detection limit. We thus conclude that the TTVs of KOI-3220.01 could be caused by a large moon, but we cannot rule out a planet.

### 5.9 TTV-TDV Correlation

As described in Kipping (2009); Heller et al. (2016), TTVs and TDVs induced by moons will show a phase difference of  $90^\circ$ . We examined all of these systems for such a shift in their TTV and TDV signals. We did not find any evidence for these signals showing such a shift though the limited number of data points and relatively high error limit what can be said in this regard.

## 6 DISCUSSION

### 6.1 Candidates Probably Devoid of Major Exomoons

KOI's 1503 and 1980 have their best-fit moons well outside of the green zone. We would then expect such moons to be easily seen in

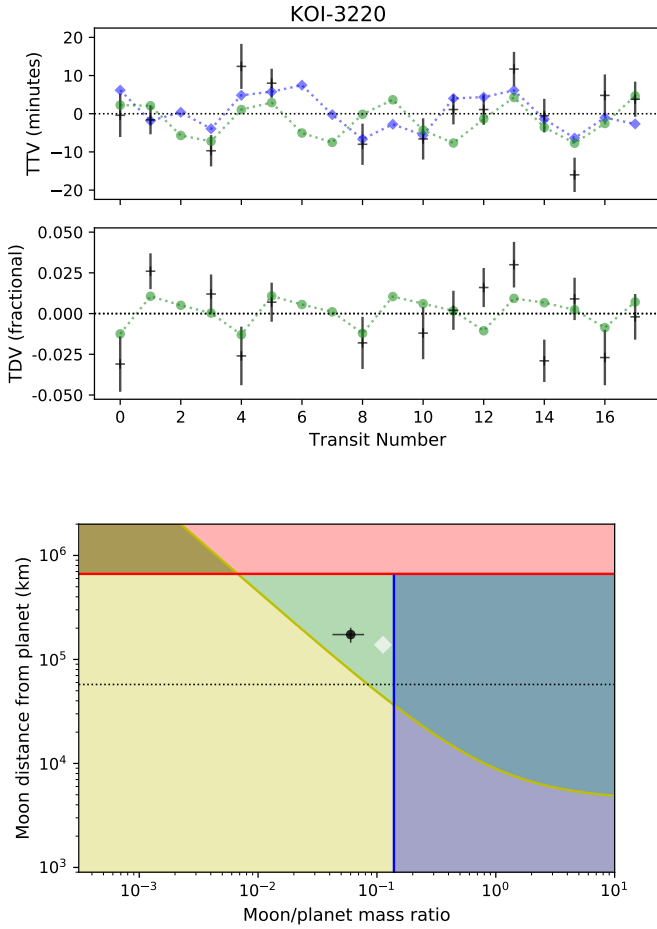


**Figure 12.** Quality of fit and sensitivity plot for KOI-3220.01. The symbols used are the same as in Figure 5.

the photometric data. Further, even if we hypothesize a moon at 0.3 Hill, the mass of these moons would need to be nearly  $1 M_{\oplus}$  to be capable of reproducing the TTV pattern. Our cursory looks at the public data (Akeson et al. 2013) shows no obvious signal in any candidate. Thus, these systems’ TTVs are probably caused by one or more other planets in the system.

## 6.2 Candidates With Possible TTV-Inducing Exomoons

The TTVs of KOI’s 268, 303, 1888, 1925, 2728 and 3220 can be plausibly explained by as-yet-unseen exomoons. Two of these systems (1888 and 1925) have best fit values right on the edge of transit detectability, but their posterior results indicate such a moon could readily be below the photometric threshold. For the remaining 4 systems, the best-fit moons and posteriors are all well inside the green zone and would not be expected to show a strong photometric transit signal. Indeed, we find no obvious indication of a moon transit in the public data from NASA’s Exoplanet Archive (Akeson et al. 2013) for any of these bodies. Other methods, such as the photodynamical modelling used by Kipping et al. (2012, 2015) could potentially provide further insights. Because each could be equally well-explained with the existence of another planet, we cannot definitively state whether there are moons present or not. However, these six systems are excellent targets for followup studies and analysis.

**Table 4.** Summary of Best-Fit Results

KOI	# Data Points	TTV SNR (min)	Planet $\chi^2/N$	Moon $\chi^2/N$	Likely Cause of TTVs
268.01	11	2.37	0.579	1.514	planet or moon
303.01	21	1.56	0.581	0.793	planet or moon
1503.01	10	1.56	0.181	0.629	planet
1888.01	12	1.84	0.883	0.682	planet or moon
1925.01	11	1.57	0.656	0.622	planet or moon
1980.01	15	1.69	0.313	0.644	planet
2728.01	20	1.71	0.427	0.748	planet or moon
3220.01	14	1.67	0.566	0.826	planet or moon

## 7 CONCLUSIONS

We examined an unexplored portion of parameter space looking for exomoons in the Kepler data. We have ruled out the existence of significant moons being the primary cause of the TTVs for two other exoplanets, KOI-1503.01 and KOI-1980.01, and establishing that those two systems likely contain another planet. However, there are TTV signals consistent with exomoons in 6 of the 8 examined systems. We cannot definitively ascribe the observed TTVs in any particular system to an exomoon, as they are equally reproducible by a hypothetical additional planet. Nonetheless, these systems warrant further examination.

## 8 ACKNOWLEDGEMENTS

This work was funded in part by the Natural Sciences and Engineering Research Council of Canada Discovery Grants program (Grant no. RGPIN-2018-05659).

## REFERENCES

- Agol E., Steffen J., Sari R., Clarkson W., 2005, *MNRAS*, **359**, 567  
Akeson R. L., et al., 2013, *Publications of the Astronomical Society of the Pacific*, **125**, 989  
Borucki W. J., et al., 2010, *Science*, **327**, 977  
Buchner J., et al., 2014, *A&A*, **564**, A125  
Chambers J. E., Wetherill G. W., Boss A. P., 1996, *Icarus*, **119**, 261  
Chen J., Kipping D. M., 2018, *MNRAS*, **473**, 2753  
Deck K. M., Agol E., Holman M. J., Nesvorný D., 2014, *ApJ*, **787**, 132  
Everhart E., 1985, in Carusi A., Valsecchi G. B., eds, *Dynamics of Comets: Their Origin and Evolution*. Springer Netherlands, Dordrecht, pp 185–202  
Feroz F., Hobson M. P., Bridges M., 2009, *MNRAS*, **398**, 1601  
Fox C., Wiegert P., 2019, *MNRAS*, **482**, 639  
Gilliland R. L., et al., 2011, *ApJS*, **197**, 6  
Gladman B., 1993, *Icarus*, **106**, 247  
Heller R., Hippke M., Placek B., Angerhausen D., Agol E., 2016, *A&A*, **591**, A67  
Heller R., Rodenbeck K., Bruno G., 2019, *A&A*, **624**, A95  
Holzer T., et al., 2016, *ApJS*, **225**, 9  
Holman M. J., Murray N. W., 2005, *Science*, **307**, 1288  
Holman M., Wiegert P., 1999, *AJ*, **117**, 621  
Kipping D. M., 2009, *MNRAS*, **392**, 181  
Kipping D. M., Bakos G. Á., Buchhave L., Nesvorný D., Schmitt A., 2012, *ApJ*, **750**, 115  
Kipping D. M., Forgan D., Hartman J., Nesvorný D., Bakos G. Á., Schmitt A., Buchhave L., 2013, *ApJ*, **777**, 134  
Kipping D. M., Nesvorný D., Buchhave L. A., Hartman J., Bakos G. Á., Schmitt A. R., 2014, *ApJ*, **784**, 28

- Kipping D. M., Schmitt A. R., Huang X., Torres G., Nesvorný D., Buchhave L. A., Hartman J., Bakos G. A., 2015, *ApJ*, **813**, 14
- Kreidberg L., Luger R., Bedell M., 2019, *ApJ*, **877**, L15
- Nicholson P. D., Cuk M., Sheppard S. S., Nesvorný D., Johnson T. V., 2008, *Irregular Satellites of the Giant Planets*. p. 411
- Sartoretti, P. Schneider, J. 1999, *Astron. Astrophys. Suppl. Ser.*, 134, 553
- Stassun K. G., Collins K. A., Gaudi B. S., 2017, *AJ*, **153**, 136
- Szabó R., Szabó G. M., Dály G., Simon A. E., Hodosán G., Kiss L. L., 2013, *A&A*, **553**, A17
- Teachey A., Kipping D. M., 2018, *Science Advances*, 4
- Wenger M., et al., 2000, *A&AS*, **143**, 9
- Wisdom J., Holman M., 1991, *AJ*, **102**, 1528

**Table 1.** Planet Hypothesis Best Fit Parameters and Posteriors

	KOI-268	KOI-303	KOI-1503	KOI-1888	KOI-1925	KOI-1980	KOI-2728	KOI-3220	
$M_b$ Best Fit	0.244	0.628	0.092	0.148	0.606	0.097	0.165	0.427	$M_J$
$M_b$ Posterior	$0.12^{+0.037}_{-0.038}$	$0.128^{+0.128}_{-0.056}$	$0.096^{+0.035}_{-0.042}$	$0.052^{+0.05}_{-0.042}$	$0.084^{+0.438}_{-0.065}$	$0.078^{+0.033}_{-0.027}$	$0.179^{+0.046}_{-0.043}$	$0.286^{+0.097}_{-0.189}$	
$P_b$ Best Fit	315.238	275.276	402.667	336.219	313.656	316.257	100.319	285.853	days
$P_b$ Posterior	$322.7^{+5.6}_{-6.1}$	$274.9^{+33}_{-18.8}$	$399.9^{+7.1}_{-8.5}$	$336.2^{+17.8}_{-8.8}$	$397.1^{+39}_{-43.2}$	$316.7^{+8.3}_{-4.8}$	$100.2^{+0.2}_{-0.3}$	$289.6^{+4.2}_{-3.6}$	
$e_b$ Best Fit	0.106	0.176	0.111	0.072	0.038	0.064	0.127	0.080	
$e_b$ Posterior	$0.042^{+0.035}_{-0.025}$	$0.215^{+0.037}_{-0.073}$	$0.06^{+0.03}_{-0.031}$	$0.078^{+0.044}_{-0.042}$	$0.128^{+0.091}_{-0.065}$	$0.055^{+0.048}_{-0.034}$	$0.094^{+0.043}_{-0.052}$	$0.036^{+0.04}_{-0.022}$	
$i_b$ Best Fit	73.017	92.891	87.610	96.091	100.355	109.623	80.521	120.846	deg
$i_b$ Posterior	$84.9^{+9.4}_{-9.1}$	$92.3^{+8.2}_{-11.6}$	$89.9^{+11.5}_{-11.3}$	$87.5^{+11.7}_{-9.3}$	$96.7^{+24.8}_{-32.9}$	$94.3^{+12.2}_{-19.4}$	$82.2^{+12.9}_{-7.8}$	$91.1^{+20.8}_{-23.1}$	
$\Omega_b$ Best Fit	-19.055	-7.919	16.590	-16.791	4.995	5.020	8.276	-42.709	deg
$\Omega_b$ Posterior	$-7.6^{+13.5}_{-9}$	$-0.5^{+7.9}_{-8.1}$	$-0.1^{+8.2}_{-9.1}$	$-1^{+13.6}_{-12.5}$	$-12^{+28.1}_{-18.7}$	$2.6^{+10.4}_{-11.1}$	$11.7^{+5.8}_{-11.8}$	$-26^{+64.7}_{-14.9}$	
$\omega_b$ Best Fit	143.035	101.62	117.472	313.707	67.048	165.781	4.665	219.65	deg
$\omega_b$ Posterior	$67^{+48}_{-38}$	$106^{+83}_{-24}$	$72^{+69}_{-41}$	$266^{+53}_{-131}$	$123^{+116}_{-76}$	$159^{+45}_{-52}$	$19^{+29}_{-14}$	$56^{+150}_{-37}$	
$Mn_b$ Best Fit	127.644	147.105	158.578	73.610	166.682	170.809	197.139	58.094	deg
$Mn_b$ Posterior	$218^{+45}_{-56}$	$151^{+71}_{-26}$	$192^{+40}_{-45}$	$107^{+68}_{-48}$	$176^{+60}_{-72}$	$175^{+51}_{-33}$	$152^{+36}_{-38}$	$237^{+36}_{-168}$	
$e_c$ Best Fit	0.021	0.003	0.112	0.104	0.149	0.065	0.090	0.050	
$e_c$ Posterior	$0.04^{+0.024}_{-0.018}$	$0.053^{+0.05}_{-0.036}$	$0.032^{+0.032}_{-0.019}$	$0.072^{+0.031}_{-0.026}$	$0.065^{+0.062}_{-0.041}$	$0.101^{+0.024}_{-0.023}$	$0.113^{+0.034}_{-0.024}$	$0.118^{+0.059}_{-0.058}$	
$\omega_c$ Best Fit	68.070	1.756	162.291	33.983	180.321	44.603	69.780	57.830	deg
$\omega_c$ Posterior	$59^{+12}_{-11}$	$349^{+5}_{-6}$	$167^{+15}_{-15}$	$42^{+11}_{-9}$	$175^{+12}_{-15}$	$39^{+15}_{-15}$	$48^{+17}_{-15}$	$46^{+9}_{-10}$	
$Mn_c$ Best Fit	19.415	87.634	299.475	46.487	286.558	40.125	16.542	29.035	deg
$Mn_c$ Posterior	$27^{+10}_{-10}$	$94^{+6}_{-6}$	$287^{+14}_{-15}$	$42^{+8}_{-8}$	$284^{+12}_{-13}$	$42^{+13}_{-12}$	$33^{+10}_{-13}$	$35^{+8}_{-8}$	
Reduced $\chi^2$ of Best Fit	0.579	0.581	0.181	0.883	0.656	0.313	0.427	0.566	

This paper has been typeset from a  $\text{\TeX}/\text{\LaTeX}$  file prepared by the author.

**Table 2.** Moon Hypothesis Best Fit Parameters and Posteriors

	KOI-268	KOI-303	KOI-1503	KOI-1888	KOI-1925	KOI-1980	KOI-2728	KOI-3220	
$M_m$ Best Fit	0.817	0.499	1.508	1.551	0.300	1.447	6.057	1.586	$M_\oplus$
$M_m$ Posterior	$0.44^{+0.09}_{-0.09}$	$0.36^{+0.1}_{-0.09}$	$0.72^{+0.35}_{-0.31}$	$1.2^{+0.32}_{-0.31}$	$0.18^{+0.05}_{-0.05}$	$0.74^{+0.26}_{-0.27}$	$4.88^{+1.02}_{-1.05}$	$0.85^{+0.27}_{-0.25}$	
$a_m$ Best Fit	0.217	0.278	0.223	0.235	0.222	0.284	0.295	0.208	$R_{Hill}$
$a_m$ Posterior	$0.257^{+0.028}_{-0.044}$	$0.277^{+0.014}_{-0.05}$	$0.24^{+0.047}_{-0.027}$	$0.285^{+0.009}_{-0.017}$	$0.276^{+0.017}_{-0.056}$	$0.252^{+0.035}_{-0.036}$	$0.289^{+0.007}_{-0.008}$	$0.261^{+0.027}_{-0.043}$	
$Mean_m$ Best Fit	89.844	321.701	81.040	257.304	238.324	265.055	35.963	17.501	deg
$Mean_m$ Posterior	$127^{+107}_{-52}$	$219^{+106}_{-124}$	$173^{+111}_{-95}$	$135^{+119}_{-95}$	$139^{+148}_{-104}$	$143^{+167}_{-113}$	$76^{+242}_{-53}$	$89^{+166}_{-58}$	
$e_m$ Best Fit	0.281	0.198	0.294	0.027	0.024	0.270	0.130	0.269	
$e_m$ Posterior	$0.122^{+0.108}_{-0.051}$	$0.113^{+0.113}_{-0.089}$	$0.175^{+0.07}_{-0.104}$	$0.053^{+0.041}_{-0.03}$	$0.07^{+0.119}_{-0.047}$	$0.141^{+0.103}_{-0.09}$	$0.051^{+0.055}_{-0.03}$	$0.136^{+0.085}_{-0.09}$	
$\omega_m$ Best Fit	101.759	82.578	265.515	48.750	207.235	219.345	246.46	210.756	deg
$\omega_m$ Posterior	$90^{+161}_{-37}$	$156^{+117}_{-102}$	$174^{+99}_{-102}$	$178^{+89}_{-113}$	$117^{+139}_{-73}$	$179^{+78}_{-72}$	$249^{+55}_{-62}$	$189^{+78}_{-105}$	
Reduced $\chi^2$ Best Fit	1.514	0.793	0.629	0.682	0.622	0.644	0.748	0.826	